HHS Public Access

Author manuscript

Exp Neurol. Author manuscript; available in PMC 2016 May 01.

Published in final edited form as:

Exp Neurol. 2015 May ; 267: 18–29. doi:10.1016/j.expneurol.2014.11.011.

Respiratory function after selective respiratory motor neuron death from intrapleural CTB–saporin injections

Nicole L. Nichols, **Stéphane Vinit**, **Lorene Bauernschmidt**, and **Gordon S. Mitchell***

Department of Comparative Biosciences, University of Wisconsin, 2015 Linden Dr., Madison, WI 53706, USA

Abstract

Amyotrophic lateral sclerosis (ALS) causes progressive motor neuron degeneration, paralysis and death by ventilatory failure. In rodent ALS models: 1) breathing capacity is preserved until late in disease progression despite major respiratory motor neuron death, suggesting unknown forms of compensatory respiratory plasticity; and 2) spinal microglia become activated in association with motor neuron cell death. Here, we report a novel experimental model to study the impact of respiratory motor neuron death on compensatory responses without many complications attendant to spontaneous motor neuron disease. In specific, we used intrapleural injections of cholera toxin B fragment conjugated to saporin (CTB–SAP) to selectively kill motor neurons with access to the pleural space. Motor neuron survival, CD11b labeling (microglia), ventilatory capacity and phrenic motor output were assessed in rats 3–28 days after intrapleural injections of: 1) CTB–SAP (25 and 50 μg), or 2) unconjugated CTB and SAP (*i.e.* control; (CTB + SAP). CTB–SAP elicited dose-dependent phrenic and intercostal motor neuron death; 7 days post-25 μg CTB–SAP, motor neuron survival approximated that in end-stage ALS rats (phrenic: 36 ± 7%; intercostal: 56 ± 10% of controls; $n = 9$; $p < 0.05$). CTB–SAP caused minimal cell death in other brainstem or spinal cord regions. CTB–SAP: 1) increased CD11b fractional area in the phrenic motor nucleus, indicating microglial activation; 2) decreased breathing during maximal chemoreceptor stimulation; and 3) diminished phrenic motor output in anesthetized rats (7 days post-25 μg, CTB–SAP: 0.3 ± 0.07 V; CTB + SAP: 1.5 ± 0.3; $n = 9$; $p < 0.05$). Intrapleural CTB–SAP represents a novel, inducible model of respiratory motor neuron death and provides an opportunity to study compensation for respiratory motor neuron loss.

Keywords

Breathing; Spinal cord; Neurodegenerative disease; Motor neuron death; Phrenic; Intercostal

Introduction

Amyotrophic lateral sclerosis (ALS) causes paralysis from progressive motor neuron degeneration, ultimately causing death from ventilatory failure. Effective means of

* Corresponding author at: Department of Comparative Biosciences, University of Wisconsin, School of Veterinary Medicine, 2015 Linden Dr., Madison, WI 53706, USA. Fax: +1 608 263 3926. mitchell@svm.vetmed.wisc.edu (G.S. Mitchell)..

preserving and/or restoring ventilatory function in ALS are necessary to improve the quality and duration of life. During disease progression in a rat model of ALS ($SOD1^{G93A}$ over-expression), signs of imminent ventilatory failure first appear as phrenic motor neuron death and decreased phrenic motor output. At this stage of disease progression, microglial cell numbers increase throughout the spinal cord, including cervical spinal regions encompassing the phrenic motor nucleus (Nikodemova et al., 2013). Increased microglial cell number is indicative of microglial activation, although the specific microglial phenotype is not easily characterized (Colton, 2009; David and Kroner, 2011; Hanisch and Kettenmann, 2007; Nikodemova et al., 2013). Since the rate, timing and extent of respiratory motor neuron death are highly variable in genetic models of ALS, we developed a novel model of *induced* respiratory motor neuron death *via* intrapleural injections of cholera toxin B fragment conjugated to the ribosomal toxin, saporin (CTB–SAP). This model will enable more controlled studies concerning the specific impact of respiratory motor neuron death on breathing.

CTB binds to the GM1 (Galactosyl-N-Acetylgalactosaminyl) receptor and is subsequently incorporated into motor neurons (Lian and Ho, 1997). Saporin is a ribosomal inactivating protein, disabling protein synthetic machinery and causing apoptotic cell death over hours to days (Llewellyn-Smith et al., 1999; Lujan et al., 2010). When CTB is conjugated to saporin (CTB–SAP), targeted cell types are eliminated whereas other cell types are unaffected (Llewellyn-Smith et al., 1999, 2000; Lujan et al., 2010). Once CTB–SAP reaches the targeted cell body, CTB and SAP dissociate, allowing saporin to inactivate ribosomes. When CTB–SAP is injected intrapleurally, motor neurons with access to the pleural space (*e.g.* phrenic) retrogradely transport it to the cell body, thereby killing the cell. Here, we report that intrapleural CTB–SAP injections simulate aspects of motor neuron degeneration previously observed in a rat model of ALS, including similar respiratory motor neuron death and its effects on the capacity to increase phrenic motor output.

Materials and methods

Animals

Experiments were conducted on adult (3–4 months old) male Sprague Dawley rats (Harlan Colony 211; Indianapolis, IN) maintained on a 12:12 light:dark cycle with *ad libitum* access to food and water. All procedures involving animals were approved by the Institutional Animal Care and Use Committee at the School of Veterinary Medicine, University of Wisconsin, and were in agreement with standards set forth in the National Institutes of Health Guide (NIH) for Care and Use of Laboratory Animals. The University of Wisconsin is accredited by AAALAC, and is covered by NIH Assurance (A3368-01).

Intrapleural injections

Cholera toxin B subunit conjugated to saporin (CTB–SAP; 25–50 μg dissolved in phosphate buffered saline (PBS); Advanced Targeting Systems; San Diego, CA) was administered intrapleurally to target respiratory motor neurons. Intrapleural injections were done according to Mantilla et al. (2009) using a 50 μL Hamilton syringe and a custom needle (6 mm, 23 gauge, semi-blunt to avoid puncturing of the lung). CTB–SAP plus extra CTB (25

or 50 μg dissolved in doubly distilled H_2O; Calbiochem; Billerica, MA; to label spared phrenic motor neurons) were bilaterally injected into the right and left pleural spaces (6 mm deep, fifth intercostal space) while the rats were under isoflurane anesthesia (1.5% isoflurane in 100% oxygen). Control rats received an injection of CTB (25–50 μg) unconjugated to saporin (SAP, 25–50 μg dissolved in PBS; Advanced Targeting Systems; San Diego, CA) or CTB + SAP as a control to demonstrate SAP alone does not cause respiratory motor neuron death. Rats were monitored for overt signs of respiratory compromise.

Plethysmography

A sub-set of rats were placed in a whole-body flow-through plethysmograph (BUXCO Electronics, Troy, NY) 7 and 28 days following intrapleural injection. This technique allows quantitative measurement of ventilation in freely-behaving rats with altered inspired gas concentrations. The system was calibrated, the rats weighed, and their body temperature was measured with a rectal thermometer (Type T Thermocouple Thermometer, Model 600-1020, Barnant Company, Barrington, IL) before being placed in the plethysmograph chamber (~2 L volume). Ventilation was assessed in control rats (CTB + SAP; 25 μg CTB + 25 μg SAP for 7 and 28 days; n = 3 each; with no differences between 7 and 28 days, control rats were grouped for analysis) and CTB–SAP (25 μg for 7 and 28 days: n = 3 each) treated rats. The rats acclimated to the chamber while breathing room air (21% O_2, balance N_2; flushed at ~3 L/min). Recording commenced once the rats were quiet but awake; ventilatory measurements were made during baseline conditions, before exposing them to 5% hypercapnia (21% O_2, 5% CO_2, balance N_2; 15 min), 7% hypercapnia (21% O_2, 7% CO_2, balance N_2; 15 min) and an hypoxic + hypercapnic gas mixture (10.5% O_2/7% CO_2; 15 min). A pressure calibration signal, plethysmograph temperature, rat body temperature, ambient and chamber pressures, and rat body mass were used to calculate breath-by-breath tidal volume (VT; Drorbaugh and Fenn, 1955; Jacky, 1978), respiratory frequency, mean inspiratory flow (VT/TI) and minute ventilation ($\dot{V}E$). VT, $\dot{V}E$ and VT/TI are reported normalized to body mass (per 100 g). Data were rejected if there was evidence of pressure fluctuations caused by gross body movements or sniffing behavior. At the conclusion of the study, rats were removed from the chambers and their body temperatures recorded.

Neurophysiological experiments

Rats were prepared as described previously (Hoffman et al., 2012; Nichols et al., 2012). Rats were induced and maintained with isoflurane (3.5% in 50% O_2, balance N_2) throughout surgical procedures. Rats were trachotomized, pump ventilated, (Rodent Ventilator, model 683; Harvard Apparatus, Holliston, MA, USA; tidal volume = 2.5 mL), and bilaterally vagotomized. A polyethylene catheter (PE50 ID: 0.58 mm, OD: 0.965 mm; Intramedic, MD, USA) was inserted into the right femoral artery to monitor blood pressure (Gould Pressure Transducer, P23ID, USA) and blood gases (ABL 800, Radiometer, Westlake, OH). A rectal thermistor (Fisher Scientific, Pittsburgh, PA, USA) was used to monitor body temperature, which was maintained (37.5 ± 1 °C) with a heated surgical table. To monitor end-tidal PCO_2 (P_{ETCO2}), a flow-through carbon dioxide analyzer was used with sufficient response time to measure P_{ETCO2} in rats (Capnogard, Novametrix, Wallingford, CT, USA). P_{ETCO2} was maintained at ~45 mm Hg throughout surgery. Phrenic nerves were isolated (dorsal

approach), cut distally, desheathed and covered with a saline soaked cotton ball until protocols commenced. Once surgery was complete, rats were converted to urethane anesthesia over 20–30 min (1.8 g kg^{-1}, *i.v.*). The adequacy of anesthesia was tested before protocols commenced, and immediately after the protocol was complete; adequacy of anesthetic depth was assessed as the lack of pressor or respiratory neural response to a toe pinch with a hemostat (Bach and Mitchell, 1996; Hoffman et al., 2012; Nichols et al., 2012). Once rats were converted to urethane, a minimum of 1 h was allowed before experiments commenced. Rats were given continuous intravenous infusions (1.5–6 mL kg^{-1} h^{-1}) of a 1:2:0.13 mixture of 6% hetastarch in 0.9% sodium chloride, lactated Ringer's solution, and 8.4% sodium bicarbonate to maintain blood volume, fluid and acid–base balance.

Experimental protocol

Phrenic nerve activity was recorded with bipolar silver electrodes, amplified (10,000×), band-pass filtered (300–10,000 Hz, Model 1800, A-M Systems, Carlsborg, WA, USA), rectified and integrated (Paynter filter, time constant, 50 ms, MA-821, CWE Inc., Ardmore, PA, USA). Integrated nerve bursts were digitized (8 kHz) and analyzed using WINDAQ data acquisition system (DATAQ Instruments, Akron, OH, USA). Rats were then paralyzed using pancuronium bromide for neuromuscular blockade to prevent spontaneous breathing efforts (2.5 mg kg^{-1}, *i.v.*) (Bach and Mitchell, 1996).

To begin protocols, the apneic threshold was determined by lowering P_{ETCO2} until nerve activity ceased for approximately 1 min. The recruit ment threshold was then determined by slowly increasing the P_{ETCO2} until nerve activity resumed (Bach and Mitchell, 1996). P_{ETCO2} was raised to ~2 mm Hg above the recruitment threshold and approximately 15–20 min were allowed to establish stable neural activity (*i.e.* baseline). Blood samples were analyzed for arterial partial pressures of O_2 (PaO_2) and CO_2 (PaCO2), and were assessed during baseline, the two hypercapnic challenges and the hypercapnic + hypoxic episode. PaO_2 was ≥150 mm Hg during baseline, and during hypercapnic challenges, but was between 35–45 mm Hg during hypercapnia + hypoxia. Following ~15–20 min of baseline, PaCO2 was set 20 mm Hg above baseline for 5 min and then PaCO2 was set 40 mm Hg above baseline for 5 min by adjusting inspired CO_2. Following the final 5 minute hypercapnic + hypoxic episode (PaCO2 was set 40 mm Hg above baseline and PaO_2 was between 35–45 mm Hg), rats were returned to baseline inspired O_2 and CO_2 levels. Phrenic motor output was assessed in control (25 μg CTB + 25 μg SAP for 3 (n = 2), 7 (n = 5) and 28 (n = 3) days; 50 μg CTB + 50 μg SAP for 14 days, n = 3; since there were no differences between control groups, all control rats were grouped for analysis) and CTB–SAP (25 μg for 3 (n = 4), 7 (n = 9) and 28 (n = 7) days; 50 μg for 7 (n = 3) and 14 (n = 3) days) treated rats.

Immunohistochemistry

At the end of neurophysiology experiments, rats were perfused transcardially with 4% paraformaldehyde in 0.1 M phosphate buffer saline (PBS, pH ~ 7.4) and the brainstem and spinal cord tissue harvested. The brainstem and spinal cord were post-fixed with 4% paraformaldehyde overnight and cryoprotected in graded sucrose (20 and 30%) at 4 °C until sinking. Transverse sections (40 μm) were cut using a freezing microtome (Leica SM 200R,

Germany) and stored at −20 °C in antifreeze solution (30% ethylene glycol, 30% glycerol and 1× PBS) until processed for motor neuron counting.

Brainstem sections containing the Nucleus Ambiguus, cervical (C3–5) and thoracic (T2–7) sections (6 per area/rat) taken from control and CTB–SAP rats were stained using immunohistochemistry techniques. Sections were separated and washed with 1× PBS three times for 5 min; each rat's tissue was contained in a separate well. To prevent non-specific antibody binding, 5% normal donkey serum (NDS), 1× PBS, and 0.2% Triton were added to each tissue sample and incubated for 30 min at room temperature. Primary antibody solution was added, consisting of 5% NDS, 1× PBS, 0.1% Triton, and the antibody against cholera toxin B subunit (CTB; goat polyclonal, 1:2000, Calbiochem; Billerica, MA) and/or CD11b (Ox42; mouse monoclonal, 1:500, AbD Serotec, Raleigh, NC). Sections were incubated overnight in the primary antibody solution on a shaker at 4 °C.

The following day, tissues were washed three times with 1× PBS (5 min each), and then incubated in the secondary antibody solution, which was composed of 5% NDS, 1× PBS, 0.1% Triton and the secondary antibody (donkey anti-goat Alexa-Fluor 594, 1:2000; Molecular Probes, Eugene, OR; and/or donkey anti-mouse Alexa-Fluor 488, 1:500; Molecu lar Probes, Eugene, OR) on a shaker for two hours in the dark at room temperature. Following incubation, tissues were washed with 1× PBS using the same procedure (3 × 5 min). Finally, sections were mounted on positively charged glass slides, covered with ProLong® Gold Antifade Reagent (Molecular Probes, Eugene, OR) to prevent quenching of fluorescence, cover-slipped and air-dried. Slides were stored at −20 °C until quantification of staining was performed using a confocal microscope at 4×, 10× and/or 20× magnification.

Motor neuron counts

Live confocal microscopy and C1–ES program software (Nikon Eclipse TE2000-U, Melville, NY) was used to quantify and take photomi crographs of Nucleus Ambiguus, phrenic and intercostal motor neurons in all brainstem and spinal cord tissues. Location of the phrenic and intercostal motor neurons in the ventral horn were determined and manually counted based on diagrams from *The Spinal Cord* (Watson et al., 2009). Specifically, phrenic motor neurons are defined as the cluster of neurons medio-lateral of the cervical ventral horn (Boulenguez et al., 2007; Mantilla et al., 2009). Surviving motor neurons were characterized as those exhibiting a CTB (+) stain, an identifiable cell body and nucleus. Right and left CTB (+) motor neurons were counted by a blinded investi gator. The number of CTB (+) motor neurons were counted from all rats in each group and compared between CTB–SAP and control rats using Microsoft Excel to allow for graphical and statistical comparisons. The number of phrenic motor neurons in the C3–5 segment was extrapolated from the 6 sections (length of the entire phrenic motor nucleus is ~2000 μm; 40 μm sections), and the number of intercostal motor neurons in the T2–7 segment was extrapolated from the 6 sections (length of segments T2–7 each was ~1000 μm; 40 μm sections). The number of phrenic motor neurons in the C3–5 segment and the number of intercostal motor neurons in the T2–7 segment were compared and there were no differences between segments, so all segments were grouped together. Phrenic motor neuron survival was assessed in control (25 μg CTB +25 μg SAP for 3 (n = 2), 7 (n = 5) and 28 (n = 3) days;

50 μg CTB + 50 μg SAP for 14 days (n = 3); since there were no differences between control rats, all control rats were grouped) and CTB–SAP (25 μg for 3 (n = 4), 7 (n = 9) and 28 (n = 7) days; 50 μg for 7 (n = 3) and 14 (n = 3) days) treated rats. Intercostal motor neuron survival was assessed in control (25 μg CTB + 25 μg SAP for 7 (n = 5) and 28 (n = 3) day; 50 μg CTB + 50 μg SAP for 14 days (n = 3); there were no differences between control rats, so all rats treated as controls were grouped) and CTB–SAP treated rats (25 μg for 3 (n = 4), 7 (n = 9) and 28 (n = 7) days; 50 μg for 7 (n = 3) and 14 (n = 3) days).

Nucleus Ambiguus motor neuron location in the brainstem were similarly determined and manually counted based on diagrams from *The Spinal Cord* (Watson et al., 2009). Specifically, Nucleus Ambiguus motor neurons are a cluster of neurons medio-lateral of the brainstem just dorsal to the ventral respiratory column and extending from bregma −14.6 mm to −11.3 mm (interaural parameters −5.6 mm to −2.3 mm; Watson et al., 2009). Surviving or healthy Nucleus Ambiguus cells were characterized as described above for spinal motor neurons. The number of Nucleus Ambiguus neurons was extrapolated from 6 sections (length of the entire Nucleus Ambiguus is ~3000 μm; 40 μm sections). Nucleus Ambiguus motor neuron survival was assessed in control (25 μg CTB + 25 μg SAP for 7 (n = 5) and 28 (n = 3) days; 50 μg CTB + 50 μg SAP for 14 days (n = 3); there were no differences between control rats, so all control rats were grouped) and CTB–SAP (25 μg for 3 (n = 4), 7 (n = 9) and 28 (n = 7) days; 50 μg for 7 (n = 3) and 14 (n = 3) days) treated rats.

CD11b image analysis

Raw images were analyzed using Image J (NIH, Bethesda, MD). Analysis was performed using images taken at 20× magnification from 2 regions of interest: 1) the phrenic motor nucleus (area surrounding CTB(+) phrenic motor neurons at spinal segments C3–5; 320.61 μm × 257.71 μm) and 2) the ventral horn at spinal segments C3–5 (700 μm × 700 μm). The fractional area occupied by CD11b label in raw image files was computed by Image J for the phrenic motor nucleus (as the percentage of the total field for the phrenic motor nucleus occupied by label positive pixels), and interpreted as the fractional area of microglia surrounding the phrenic motor nucleus. The fractional area occupied by CD11b label in raw image files was calculated manually for the non-phrenic ventral horn. Total label positive pixels were determined for the phrenic motor nucleus (fractional area multi plied by total pixels in the phrenic motor nucleus) and for the ventral horn (fractional area multiplied by total pixels in the ventral horn). Total label positive pixels for the non-phrenic ventral horn were deter mined by subtracting total label positive pixels in the phrenic motor nucleus from those in the ventral horn. Total label positive pixels for the non-phrenic ventral horn were then divided by the total pixels of the non-phrenic ventral horn (total pixels of the phrenic motor nucleus was subtracted from the total pixels in the ventral horn). Increased fractional area of CD11b staining indicates microglial activation (Ling and Wong, 1993; Ling et al., 1990; Robinson et al., 1986; Roy et al., 2006; Windelborn and Mitchell, 2012). This analysis does not allow distinction between greater cell size *vs.* cell number. CD11b fractional area on both sides in the phrenic motor nucleus and non-phrenic ventral horn for all rats in each group were compared between CTB–SAP and control rats. CD11b fractional area was assessed in control (25 μg CTB + 25 μg SAP for 7 (n = 5) and 28 (n = 3) days; 50 μg CTB + 50 μg SAP for 14 days (n = 3); there were no differences between control groups, so they

were grouped in the analysis) and CTB–SAP (25 μg for 3 (n = 4), 7 (n = 9) and 28 (n = 7) days; 50 μg for 7 (n = 3) and 14 (n = 3) days) treated rats.

Analysis

Plethysmography, apneic and recruitment thresholds, and integrated phrenic nerve burst amplitude data were compared with a two-way repeated measures ANOVA, with group (control vs. CTB–SAP) and level (baseline *etc.* or threshold) as factors. There were no differences in animals injected with control or in animals injected with CTB–SAP for apneic and recruitment thresholds, so thresholds were combined for all control and CTB–SAP treated rats. Integrated phrenic nerve burst ampli tudes were averaged over 1 min during baseline, during the two hypercapnic challenges and during the hypercapnia + hypoxia challenge. Only baseline and hypercapnia + hypoxia data are reported for both plethysmography and integrated phrenic nerve burst amplitudes. Phrenic nerve burst amplitude is reported as the voltage of the integrated signal (*i.e.* arbitrary units). Statistical comparisons between treatment groups for phrenic nerve burst amplitude were done using a one-way ANOVA to compare baseline values or the hypercapnia + hypoxia challenge across treatment groups (the results of this analysis did not differ from the results of the two-way repeated measures ANOVA; since fundamental conclusions were the same, we report phrenic nerve burst data during baseline and hypercapnia + hypoxia separately to increase clarity). For histological analysis, a one-way ANOVA was used to compare motor neuron survival and CD11b fractional area within and across control and CTB–SAP treatment groups. If significant differences were indicated, individual comparisons were made using a Fisher's least significant difference (LSD) *post hoc* test (Sigma Plot version 12.0; Systat Software Inc., San Jose, CA, USA). All differences between groups were considered significant if $p < 0.05$; all values are expressed as means ± 1 S.E.M. Multiple linear regression analyses were performed between baseline or maximal phrenic activity with phrenic motor neuron survival, baseline or maximal VT/100 g with phrenic motor neuron survival, baseline or maximal VT/100 g with baseline or maximal phrenic activity, and baseline or maximal VT/100 g with intercostal motor neuron survival.

Results

Phrenic motor neurons are killed by CTB–SAP

Intrapleural injections target motor neurons with access to the pleural space, including cervical phrenic motor neurons. Representative photo- micrographs of CTB labeled phrenic motor neurons from the C3–5 spinal ventral horn from a control and 25 μg CTB–SAP treated rat (7 days) are depicted in Figs. 1 (A–F). Phrenic motor neuron numbers were decreased in all CTB–SAP treated vs. control rats, where control rats had 203 ± 18 neurons (Fig. 1G; $p < 0.05$). Average phrenic motor neuron survival counts following 25 μg CTB–SAP injections were: 3 days: 131 ± 34, 7 days: 73 ± 14, 28 days: 33 ± 13 (Fig. 1G; all $p < 0.05$ vs. control). Survival counts following 50 μg CTB–SAP injection were: 7 days: 33 ± 5, 14: days 0.5 ± 0.5 (Fig. 1G; all $p < 0.05$ *vs.* control). 25 μg CTB–SAP at 3 days post-injection had significantly less phrenic motor neuron death *versus* other CTB–SAP treated rats; rats treated with 25 μg CTB–SAP had significantly less phrenic motor neuron death at 7

days *versus* rats treated with 50 μg CTB–SAP for 14 days (Fig. 1 G; $p < 0.05$). Thus, intrapleural CTB–SAP kills phrenic motor neurons.

Intercostal motor neurons are killed by CTB–SAP

Intercostal motor neurons also access the pleural space and, thus, are exposed to CTB–SAP. Representative photomicrographs of CTB labeled intercostal motor neurons from the T2–7 spinal ventral horn from a control rat and a rat treated with 25 μg CTB–SAP (7 days) are depicted in Figs. 2 (A–F). In the intermediolateral cell column of T2–7 (a non- targeted area giving rise to sympathetic preganglionic fibers; Bennett et al., 1986), there was a lack of staining in either control or CTB–SAP treated rats (yellow arrows in Figs. 2A, D). Intercostal motor neurons numbers were decreased in all CTB–SAP treated *vs.* control rats. Control rats had 509 ± 48 intercostal motor neurons in the ventral horn (Fig. 2G; $p < 0.05$). Average intercostal motor neuron survival counts following 25 μg CTB–SAP injection were: 3 days: 322 ± 102, 7 days: 284 ± 53, 28 days: 66 ± 27 (Fig. 2G; all $p < 0.05$ *vs.* control). Survival counts following 50 μg CTB–SAP injection were: 7 days: 25 ± 12, 14 days: 8 ± 4 (Fig. 2G; all $p < 0.05$ *vs.* control). Three days after intrapleural injection of 25 μg CTB–SAP, intercostal motor neuron survival was greater than in CTB–SAP treated rats with 25 μg at 28 days and 50 μg at 7 or 14 days. Rats treated with 25 μg CTB–SAP (7 days) had significantly more intercostal motor neurons *versus* rats treated with 25 μg CTB–SAP at 28 days and 50 μg CTB–SAP at 7 or 14 days (Fig. 2 G; $p < 0.05$). Thus, CTB–SAP targets and kills intercostal motor neurons.

Phrenic motor neuron output is decreased in CTB–SAP treated rats

CO_2 apneic and recruitment thresholds were unaffected by CTB–SAP (apneic threshold: control = 37.4 ± 0.7 mm Hg *vs.* CTB–SAP = 37.4 ± 0.5 mm Hg; recruitment threshold: control 45.6 ± 0.9 mm Hg *vs.* CTB–SAP = 46.4 ± 0.6 mm Hg; both p N 0.05). Phrenic motor output during baseline and with graded chemoreceptor stimulation in a control and CTB–SAP treated rats is illustrated in Fig. 3. Representative traces of compressed, integrated phrenic neurograms in control rats and rats following 25 or 50 μg CTB–SAP are depicted in Fig. 3A. In CTB–SAP treated rats, phrenic motor output was significantly decreased during baseline (25 μg 3 days: 0.7 ± 0.2 V; 25 μg 7 days: 0.3 ± 0.07 V; 25 μg 28 days: 0.3 ± 0.08; 50 μg 7 days: 0.01 ± 0.01 V; 50 μg 14 days: 0.05 ± 0.02 V; Fig. 3B) and maximal chemoreceptor stimulation (hypercapnia + hypoxia; 25 μg 3 days: 1.2 ± 0.3 V; 25 μg 7 days: 1.0 ± 0.2 V; 25 μg 28 days: 1.0 ± 0.3; 50 μg 7 days: 0.04 ± 0.02 V; 50 μg 14 days: 0.08 ± 0.04 V; Fig. 3C) *versus* controls (1.7 ± 0.2 V, baseline; 2.9 ± 0.3 V, maximum chemoreceptor stimulation) (Figs. 3B, C; $p < 0.05$). 7-days post 25 μg of CTB–SAP is similar to the impairment of phrenic motor neuron output in $SOD1^{G93A}$ rats at end-stage (~0.4 V; Nichols et al., 2013a).

Ventilatory capacity is decreased in CTB–SAP treated rats

Respiratory variables were studied *via* plethysmography during baseline and graded chemoreceptor stimulation in unanesthetized control and 25 μg CTB–SAP rats at 7 and 28 days post-treatment. All respiratory variables increased from baseline to hypercapnia + hypoxia (Fig. 4; $p < 0.05$). On the other hand, VT was unaffected by CTB–SAP at baseline

(1.1 ± 0.09 mL/100 g, 7 days; 0.9 ± 0.05 mL/ 100 g, 28 days; $p > 0.05$ *vs.* control), but was decreased during hypercapnia + hypoxia in CTB–SAP treated rats (1.8 ± 0.39 mL/100 g, 7 days; 1.4 ± 0.19 mL/100 g, 28 days; $p < 0.05$) *versus* controls (1.1 ± 0.04 mL/ 100 g, baseline; 2.4 ± 0.14 mL/100 g; Fig. 4A). Baseline frequency increased in rats treated with 25 μg CTB–SAP at 28 days (116 ± 11 breaths/min; $p < 0.05$ *vs.* control), but not at 7 days post-injection (94 ± 26 breaths/min; $p = 0.073$ *vs.* control: 68 ± 5 breaths/min; Fig. 4B). Frequency during hypercapnia + hypoxia was unaffected when comparing CTB–SAP (150 ± 15 breaths/min, 7 days; 169 ± 5 breaths/min, 28 days) and control rats (147 ± 2 breaths/min; Fig. 4B; $p > 0.05$). $\dot{V}E$ and VT/TI were unaffected in rats treated with CTB–SAP at baseline ($\dot{V}E$: 99 ± 23 mL/min/100 g, 7 days; 102 ± 11 mL/min/ 100 g, 28 days; VT/TI: 4.7 ± 0.6 mL/s/100 g, 7 days; 5.1 ± 0.5 mL/s/ 100 g, 28 days; $p < 0.05$ *vs.* control), but were decreased during hypercapnia + hypoxia in CTB–SAP treated rats ($\dot{V}E$: 264 ± 43 mL/min/100 g, 7 days; 231 ± 31 mL/min/100 g, 28 days; VT/TI: 10 ± 1.7 mL/s/100 g, 7 days; 8.7 ± 1.3 mL/s/100 g, 28 days; $p < 0.05$) *versus* controls ($\dot{V}E$: 70 ± 4 mL/min/100 g, baseline; 348 ± 19 mL/min/100 g, hypercapnia + hypoxia; VT/TI: 4.0 ± 0.2 mL/s/100 g, baseline; 13 ± 0.8 mL/s/100 g, hypercapnia + hypoxia; Figs. 4C, D). Thus, CTB–SAP treatment does not affect baseline ventilatory volumes, but decreases the ventilatory response to maximal chemoreceptor stimulation.

Correlations between phrenic motor output, motor neuron survival and ventilation

Multiple regression analyses were performed, including baseline or maximal (hypercapnia + hypoxia) phrenic output with phrenic motor neuron survival (Figs. 5A, B); baseline or maximal VT/100 g with phrenic motor neuron survival (Figs. 5C, D); baseline or maximal VT/100 g with baseline or maximal phrenic output (Figs. 5E, F); and baseline or maximal VT/100 g with intercostal motor neuron survival (Figs. 5G, H). Significant positive correlations were detected between: 1) baseline and maximal phrenic output with phrenic motor neuron survival (base line: slope = 0.05; $R^2 = 0.56$; maximum: slope = 0.46; $R^2 = 0.45$; both $p < 0.001$; Figs. 5A, B); 2) maximal VT/100 g with phrenic motor neuron survival (slope = 1.6; $R^2 = 0.41$; $p = 0.025$; Fig. 5D); and 3) maximal VT/100 g with maximal phrenic output (slope = 1.5; $R^2 = 0.6$; $p = 0.003$; Fig. 5F). Thus, phrenic motor neuron survival predicts phrenic motor output and max VT/100 g; further, maximal phrenic motor output predicts maximal VT/100 g. Although phrenic motor neuron survival and maximal phrenic motor output predict maximal VT/ 100 g, this effect is not sufficient to account for all of the deficits in maximal VT/100 g (Fig. 5) since the slope is not 1, and there is consid erable variability in the regression (reflected in the R^2 value below 1).

Initial multiple regression analysis was done by assessing correlations between baseline and maximal VT/100 g *versus* both phrenic and inter- costal motor neuron survival. In these analyses, there was a marginal correlation between maximal VT/100 g and intercostal motor neuron survival ($p = 0.075$; coefficient = 0.0015) *vs.* phrenic motor neuron sur vival ($p = 0.696$; coefficient = 0.00078). Thus, intercostal motor neuron survival was a stronger predictor of maximal VT/100 g than phrenic motor neuron survival. When intercostal motor neuron survival was removed from the regression, the p-value became significant between maximal VT/100 g and phrenic motor neuron survival ($p = 0.025$; coefficient = 0.0038; Fig. 5D). When phrenic motor neuron survival was removed from the regression, the correlation

between maximal VT/100 g and intercostal motor neuron survival became significant (coefficient = 0.0017; slope = 1.4; R^2 = 0.59; p = 0.004; Fig. 5H). Thus, intercostal motor neuron survival better predicts maximal

Nucleus Ambiguus motor neurons are not affected by intrapleural CTB–SAP

Since non-targeted cell death is possible using this technique, relevant brainstem areas were assessed, including the Nucleus Ambiguus. There was abundant and consistent staining in the Nucleus Ambiguus in control and CTB–SAP treated rats (Figs. 6A, B). However, there was a lack of staining in sections examined from the entire rostrocaudal extent of the area just ventral and/or ventromedial to the Nucleus Ambiguus, a region corresponding to the ventral respiratory column (a bilateral column of respiratory-related neurons known to be active during different phases of the breathing cycle that generates/modulates breathing rhythm and pattern; Onimaru et al., 1987; Smith et al., 1991; Bryant et al., 1993; Feldman et al., 2009; McCrimmon et al., 2009; Mitchell et al., 2009; Smith et al., 2009) (see Figs. 6A, B). The presence of ventral respiratory column neurons within the specific brainstem sections observed was verified by NeuN counterstaining (data not shown). Nucleus Ambiguus motor neuron counts were unchanged by CTB–SAP *versus* control rats (Control: 424 ± 73; 25 μg CTB–SAP 3 days: 525 ± 75; 25 μg 7 days: 274 ± 73; 25 μg 28 days: 449 ± 81; 50 μg CTB–SAP 7 days: 431 ± 169; 50 μg CTB–SAP 14 days: 95 ± 15; Fig. 6C; p = 0.128). However, in rats 14 days post-50 μg CTB–SAP, Nucleus Ambiguus motor neuron counts were significantly decreased if compared only with control rats (p = 0.042), suggesting marginal statistical significance. Thus, it may be suggested that NA motor neuron death occurs only with higher doses and/or longer durations post-injection. There were no apparent effects of CTB–SAP treatment in other brainstem areas, including the lateral reticular nucleus, gigantocellular reticular nucleus and the lateral paragigantocellular nucleus (data not shown; areas located based on diagrams from *The Spinal Cord* by Watson et al., 2009). The “trace” staining patterns observed are consistent with reports after CTB injections into the upper lung lobe, or pseudorabies virus injections into the lung or trachea (Dehkordi et al., 2006; Fontan et al., 2000; Hadziefendic and Haxhiu, 1999; Haxhiu et al., 1993; Zaidi et al., 2005).

CD11b fractional area is increased in the phrenic motor nucleus by CTB–SAP

Spinal microglial number increases with disease progression in $SOD1^{G93A}$ rats (Nikodemova et al., 2013). Since a major goal in developing the CTB–SAP model was to mimic key aspects of motor neuron disease, we studied microglial activation after CTB–SAP by using the well-known microglial marker, CD11b. CD11b fractional area was analyzed near the phrenic motor nucleus between C3 to C5, and in the non-phrenic ventral horn (*i.e.* the area of ventral horn excluding the phrenic motor nucleus). CD11b staining was markedly increased near the phrenic motor nucleus after CTB–SAP (Figs. 7A, B); CD11b fractional area in the phrenic motor nucleus was increased in all CTB–SAP treated *versus* control rats (Control, 32 ± 6%; 25 μg CTB–SAP 3 days, 73 ± 12%; 25 μg CTB–SAP 7 days, 58 ± 7%; 25 μg CTB–SAP 28 days, 58 ± 12%; 50 μg CTB–SAP 7 days, 70 ± 8%; 50 μg 14 days, 70 ± 11%; Fig. 7C; all $p < 0.05$ *vs.* control). Within the non-phrenic region of the C3–5 ventral horn, CD11b fractional area was increased only in 25 μg CTB–SAP treated rats at 3 days (Control, 22 ± 5%; 25 μg CTB–SAP 3 days, 65 ± 15%; 25 μg CTB–SAP 7 days, 43 ±

7%; 25 μg CTB–SAP 28 days, 44 ± 12%; 50 μg CTB–SAP 7 days, 52 ± 8%; 50 μg 14 days, 46 ± 14%; Fig. 7D; $p < 0.05$ when comparing 25 μg 3 days *vs.* control). Thus, CD11b fractional area was uniquely increased in the phrenic motor nucleus after CTB–SAP, indicating microglial activation that is superficially similar to the activation observed at disease end-stage in $SOD1^{G93A}$ rats (Nikodemova et al., 2013).

Discussion

The main findings of this study are that intrapleural CTB–SAP elicits: 1) targeted respiratory motor neuron death (phrenic and intercostal); 2) decreased phrenic motor output; 3) decreased breathing capacity during maximal chemoreceptor stimulation; 4) microglial activation near dead/dying phrenic motor neurons (but not in the adjacent ventral horn); and 5) minimal off-target cell death. Although major respiratory motor neuron cell death was accompanied by decreased phrenic motor output and breathing capacity during maximal chemoreceptor stimula tion with CTB–SAP, rats still managed to compensate sufficiently to sustain baseline breathing. CTB–SAP treated rats may compensate for loss of respiratory motor neurons *via* mechanisms similar to $SOD1^{G93A}$ rats (Nichols et al., 2013a, 2013b). Thus, intrapleural CTB–SAP represents a novel, inducible and controllable model to study motor neuron disease.

How do CTB–SAP treated rats breathe despite major respiratory motor neuron death?

CTB–SAP treatment killed both phrenic and intercostal motor neurons and decreased phrenic motor output, causing deficits in ventilatory capacity (Figs. 1, 2, 3 and 4). Nevertheless, loss of function (breathing) was not proportionate to the amount of cell death, suggesting that CTB–SAP induced cell death elicits mechanisms of compensatory respiratory plasticity. Significant positive correlations between baseline and maximal phrenic output with phrenic motor neuron survival (Figs. 5A, B), maximal VT with phrenic motor neuron survival (Fig. 5D), and maximal VT with maximal phrenic output (Fig. 5F) indicate functional impairment; however the coefficients (slopes) in each case are less than one (Fig. 5D), indicating disproportionate (lesser) impairment relative to motor neuron death. Unknown mechanisms must preserve function at a level greater than predicted from motor neuron loss. Such compensa tion may arise from: 1) recruitment of spared phrenic motor neurons that are not normally active during breathing; 2) synaptic plasticity onto spared respiratory motor neurons; 3) motor end-plate sprouting, creating larger functional motor units in respiratory muscles; and/or 4) shifting the balance of respiratory muscle contributions so that less affected, accessory respiratory muscles contribute more to the act of breathing.

Positive correlations between intercostal motor neuron survival and maximal VT (Fig. 5H) suggest that this motor pool actively contributes more to breathing after CTB–SAP. Although mammalian breathing is typically thought to be driven primarily by the diaphragm (*i.e.* phrenic motor neurons; Feldman et al., 2009), other respiratory muscles such as the intercostals contribute more to ventilation during elevated respiratory drive, lung disease or after bilateral phrenicotomy (Mitchell et al., 2009; Navarrete-Opazo and Mitchell, 2014; Sherrey and Megirian, 1990). This concept is consistent with correlations between surviving

intercostal motor neuron numbers and maximal VT (Fig. 5H). However, we did not assess intercostal motor output in this study and, thus, cannot rule out contributions from other populations of respiratory motor neurons.

Mechanisms of spontaneous compensation in response to respiratory motor neuron death in CTB–SAP treated (or ALS) rats remain to be determined, and warrant further investigation. Possible mechanisms include increased recruitment of respiratory muscles that do not have access to the pleural space, including but not limited to the scalenes, sternocleidomastoids, trapezius, iliocostalis and serratus muscles. Neuro-muscular junctions may sprout forming larger motor units, functionally assuming the role of lost motor neurons. Further, synaptic vesicle pool size at diaphragm neuromuscular junctions may increase, strengthening the motor end plate similar to the response following cervical spinal injury (Mantilla and Sieck, 2009; Mantilla et al., 2007). Finally, there may be central neural plasticity, increasing synaptic drive to spared motor neurons, driving greater contributions to the ongoing motor task (breathing).

Conversely, diaphragm atrophy may be expected following CTB–SAP. Diaphragm atrophy occurs rapidly with diminished muscular contraction, such as during mechanical ventilation (Levine et al., 2008; Powers et al., 2009), denervation (Aravamudan et al., 2006; Sieck, 1994), or with clinical disorders such as COPD (Levine et al., 2013; Mantilla and Sieck, 2013), cervical spinal injury (Mantilla et al., 2013) and ALS (de Carvalho et al., 1996; Llado et al., 2006). Subsequent loss of diaphragm force generating capacity is expected to exacerbate functional deficits, requiring yet greater compensation to preserve breathing.

Minimal non-targeted cell death after CTB–SAP

We observed similar (minimal) brainstem staining in control and CTB–SAP treated rats (Fig. 6). Intrapleural CTB and CTB–SAP injections may gain access to the brainstem *via* vagal efferent neurons that travel in this space en route to cardiac and pulmonary viscera (Grélot et al., 1989; Kalia, 1981; Kalia and Sullivan, 1982). Thus, CTB and CTB–SAP staining in the Nucleus Ambiguus likely reflects retrograde transport along these preganglionic efferents to airway-related vagal preganglionic neurons. A similar pattern of labeling was reported when CTB or pseudorabies virus is injected into the lung or trachea (Dehkordi et al., 2006; Fontan et al., 2000; Hadziefendic and Haxhiu, 1999; Haxhiu et al., 1993; Zaidi et al., 2005). Further, second order neurons in the gigantocellular reticular nucleus and the lateral paragigantocellular nucleus innervate airway-related vagal preganglionic neurons (Hadziefendic and Haxhiu, 1999; Zaidi et al., 2005). In agreement, we observed some staining in the lateral reticular nucleus, gigantocellular reticular nucleus and the lateral paragigantocellular nucleus (data not shown). Second order neurons in the gigantocellular reticular nucleus and the lateral paragigantocellular nucleus may have been retrogradely stained from neurons in the Nucleus Ambiguus. Staining was also observed in the lateral reticular nucleus, an area known to receive inputs from the vagus nerves (Perrin and Crousillat, 1983). Although staining was observed in non-targeted brainstem areas, it was similar between control and CTB–SAP treated rats (with the exception of rats 14 days after the higher dose studied); minimal cell death may have occurred in these brainstem areas since CTB and CTB–SAP were retrogradely transported a greater distance (brainstem

versus spinal cord), requiring higher doses and longer durations before cell death could be observed. Thus, 25 μg CTB–SAP seems more appropriate as a model to assure selective targeting of respiratory alpha-motor neurons.

Microglial activation in CTB–SAP treated rats

Microglial activation in the phrenic motor nucleus after CTB–SAP (Fig. 7) is consistent with microglial reaction to motor neuron cell death. CD11b fractional area may have increased due to proliferation, migration and/or cell enlargement, as observed following ischemic injury (Ferrazzano et al., 2013; Shi et al., 2011). Since our limited analysis does not allow differentiation between microglial phenotypes (Colton, 2009; David and Kroner, 2011; Hanisch and Kettenmann, 2007; Nikodemova et al., 2013), we do not know if CTB–SAP microglial activation is beneficial or detrimental. Since systemic and neuro-inflammation both increase breathing frequency at rest and impair breathing capacity during chemoreflex activation (Huxtable et al., 2011, 2013; Vinit et al., 2011), activated microglia may impair breathing capacity in CTB–SAP rats. This possibility awaits further investigation. Superficially, the CTB–SAP model mimics microglial number during end-stage motor neuron disease in $SOD1^{G93A}$ rats.

Significance

Intrapleural CTB–SAP elicits selective (targeted) respiratory motor neuron cell death and, in this respect, mimics aspects of progressive motor neuron degeneration in ALS. Although the pathogenesis of motor neuron death is different in ALS *versus* CTB–SAP, functional impairment of phrenic motor output and breathing capacity (although significant) is not as severe as expected based on respiratory motor neuron loss in either model. Thus, intrapleural CTB–SAP injections represent a novel inducible and reproducible model to study the impact of respiratory motor neuron death on breathing without many of the complications attendant to rodent models of ALS (variable motor neuron death, uncontrolled rate and onset of cell death, *etc*.). Ongoing investigations are designed to define mechanisms of spontaneous and induced (acute intermittent hypoxia) respiratory motor plasticity and their ability to keep rats breathing and alive despite impressive respiratory motor neuron cell death.

Enhanced phrenic long-term facilitation occurs in end-stage $SOD1^{G93A}$ rats (Nichols et al., 2013a), although the mechanism triggering this enhancement is unknown. The CTB–SAP model will enable tests of the hypothesis that motor neuron cell death *per se* is the proximate cause of enhanced phrenic long-term facilitation. Enhanced plasticity in motor neuron disease is of considerable significance given the ability to restore lost motor function with procedures as simple as a single exposure to acute intermittent hypoxia (Nichols et al., 2013a). Indeed, repetitive intermittent hypoxia may be useful as a tool to treat ALS patients when ventilatory failure is at hand. Given this, an understanding of mechanisms preserving and enhancing phrenic long-term facilitation in $SOD1^{G93A}$ rats is of considerable importance.

Since most ALS patients develop respiratory insufficiency, leading to ventilator dependence and/or death, an important long-range goal is to develop new strategies to delay respiratory motor neuron death and enhance the functional capacity of spared respiratory motor

neurons. Thus, understanding triggers for enhanced plasticity during motor neuron death may allow us to harness mechanisms of respiratory motor plasticity to increase/preserve the function of surviving motor neurons. These novel strategies, if successful, may guide future translational studies in patients suffering from respiratory motor neuron death, including ALS and spinal muscular atrophy. The present studies may also have wide reaching benefits for non- respiratory motor pools since repetitive intermittent hypoxia improves limb function in rodents (Lovett-Barr et al., 2012) and humans (Hayes et al., 2014; Trumbower et al., 2012) with chronic, incomplete spinal injury. Thus, our studies may reflect general properties of motor systems, and suggest novel strategies to treat non-respiratory motor disorders (Dale et al., 2014).

Acknowledgments

The authors thank Kellie Bowen for contributing to the ideas stimulating this study, Rebecca Johnson for careful critique of the manuscript, Kalen Nichols for assistance with blood–gas analysis, and Natalie Morgan and Latoya Allen for assistance with immunohistochemistry experiments. This work was supported by NIH R01 HL080209, K99 HL119606 (NLN) and T35 0D011078-04 (LB), the Francis Families Foundation (NLN), and the Craig H. Neilsen Foundation (SV).

Abbreviations

ALS	amyotrophiclateralsclerosis
AIH	acuteintermittenthypoxia
pLTF	phrenic long-term facilitation
CTB	choleratoxin B
CTB–SAP	cholera toxin B conjugated to saporin
VT	tidal volume
VT/TI	mean inspiratory flow
VE	minute ventilation
$\mathbf{P_{ETCO2}}$	partial pressure of end-tidal carbon dioxide
PaCO2	partial pressure of arterial carbon dioxide
PaO	partial pressure of arterial oxygen

References

Aravamudan B, Mantilla CB, Zhan WZ, Sieck GC. Denervation effects on myonuclear domain size of rat diaphragm fibers. J. Appl. Physiol. 2006; 100(5):1617–1622. [PubMed: 16410375]

Bach KB, Mitchell GS. Hypoxia-induced long-term facilitation of respiratory activity is serotonin dependent. Respir. Physiol. 1996; 104:251–260. [PubMed: 8893371]

Bennett JA, Goodchild CS, Kidd C, McWilliam PN. The location and characteristics of sympathetic preganglionic neurones in the lower thoracic spinal cord of dog and cat. Q. J. Exp. Physiol. 1986; 71(1):79–92. [PubMed: 3952264]

Boulenguez P, Gestreau C, Vinit S, Stamegna JC, Kastner A, Gauthier P. Specific and artifactual labeling in the rat spinal cord and medulla after injection of monosynaptic retrograde tracers into the diaphragm. Neurosci. Lett. 2007; 417(2):206–211. [PubMed: 17412505]

Bryant TH, Yoshida S, de Castro D, Lipski J. Expiratory neurons of the Bötzinger Complex in the rat: a morphological study following intracellular labeling with biocytin. J. Comp. Neurol. 1993; 335(2):267–282. [PubMed: 8227518]

Colton CA. Heterogeneity of microglial activation in the innate immune response in the brain. J. NeuroImmune Pharmacol. 2009; 4(4):399–418. [PubMed: 19655259]

Dale EA, Ben Mabrouk F, Mitchell GS. Unexpected benefits of intermittent hypoxia: enhanced respiratory and nonrespiratory motor function. Physiology. 2014; 29(1):39–48. [PubMed: 24382870]

David S, Kroner A. Repertoire of microglial and macrophage responses after spinal cord injury. Nat. Rev. Neurosci. 2011; 12(7):388–399. [PubMed: 21673720]

de Carvalho M, Matias T, Coelho F, Evangelista T, Pinto A, Luis ML. Motor neuron disease presenting with respiratory failure. J. Neurol. Sci. 1996; 139(Suppl.):117–122. [PubMed: 8899670]

Dehkordi O, Kc P, Balan KV, Haxhiu MA. Airway-related vagal preganglionic neurons express multiple nicotinic acetylcholine receptor subunits. Auton. Neurosci. 2006; 128(1–2):53–63. [PubMed: 16616705]

Drorbaugh JE, Fenn WO. A barometric method for measuring ventilation in newborn infants. Pediatrics. 1955; 16:81–87. [PubMed: 14394741]

Feldman, JL.; McCrimmon, DR.; Mitchell, GS.; Del Negro, C. Generation of respiratory rhythm in mammals.. In: Squire, LR., editor. Encyclopedia of Neuroscience. Academic Press; Oxford: 2009. p. 463-470.

Ferrazzano P, Chanana V, Uluc K, Fidan E, Akture E, Kintner DB, Cengiz P, Sun D. Age-dependent microglial activation in immature brains after hypoxia–ischemia. CNS Neurol. Disord. Drug Targets. 2013; 12(3):338–349. [PubMed: 23469850]

Fontan JJ, Diec CT, Velloff CR. Bilateral distribution of vagal motor and sensory nerve fibers in the rat's lungs and airways. Am. J. Physiol. Regul. Integr. Comp. Physiol. 2000; 279(2):R713–R728. [PubMed: 10938263]

Grélot L, Barillot JC, Bianchi AL. Central distributions of the efferent and afferent components of the pharyngeal branches of the vagus and glossopharyngeal nerves: an HRP study in the cat. Exp. Brain Res. 1989; 78(2):327–335. [PubMed: 2599042]

Hadziefendic S, Haxhiu MA. CNS innervation of vagal preganglionic neurons controlling peripheral airways: a transneuronal labeling study using pseudorabies virus. J. Auton. Nerv. Syst. 1999; 76(2–3):135–145. [PubMed: 10412837]

Hanisch UK, Kettenmann H. Microglia: active sensor and versatile effector cells in the normal and pathologic brain. Nat. Neurosci. 2007; 10(11):1387–1394. [PubMed: 17965659]

Haxhiu MA, Jansen AS, Cherniack NS, Loewy AD. CNS innervation of airway- related parasympathetic preganglionic neurons: a transneuronal labeling study using pseudorabies virus. Brain Res. 1993; 618(1):115–134. [PubMed: 8402166]

Hayes HB, Jayaraman A, Herrmann M, Mitchell GS, Rymer WZ, Trumbower RD. Daily intermittent hypoxia enhances walking after chronic spinal cord injury: a randomized trial. Neurology. 2014; 82(2):104–113. [PubMed: 24285617]

Hoffman MS, Nichols NL, MacFarlane PM, Mitchell GS. Phrenic long-term facilitation after acute intermittent hypoxia requires spinal ERK activation but not TrkB synthesis. J. Appl. Physiol. 2012; 113(8):1184–1193. [PubMed: 22961271]

Huxtable AG, Vinit S, Windelborn JA, Crader SM, Guenther CH, Watters JJ, Mitchell GS. Systemic inflammation impairs respiratory chemoreflexes and plasticity. Respir. Physiol. Neurobiol. 2011; 178(3):482–489. [PubMed: 21729770]

Huxtable AG, Smith SM, Vinit S, Watters JJ, Mitchell GS. Systemic LPS induces inflammatory gene expression and impairs phrenic long-term facilitation following acute intermittent hypoxia. J. Appl. Physiol. 2013; 114(7):879–887. [PubMed: 23329821]

Jacky JP. A plethysmograph for long-term measurements of ventilation in unrestrained animals. J. Appl. Physiol. 1978; 45(4):644–647. [PubMed: 101497]

Kalia M. Brain stem localization of vagal preganglionic neurons. J. Auton. Nerv. Syst. 1981; 3(2–4): 451–481. [PubMed: 7276442]

Kalia M, Sullivan JM. Brainstem projections of sensory and motor components of the vagus nerve in the rat. J. Comp. Neurol. 1982; 211(3):248–265. [PubMed: 7174893]

Levine S, Nguyen T, Taylor N, Friscia ME, Budak MT, Rothenberg P, Zhu J, Sachdeva R, Sonnad S, Kaiser LR, Rubinstein NA, Powers SK, Shrager JB. Rapid disuse atrophy of diaphragm fibers in mechanically ventilated humans. 2008

Levine S, Bashir MH, Clanton TL, Powers SK, Singhal S. COPD elicits remodeling of the diaphragm and vastus lateralis muscles in humans. J. Appl. Physiol. 2013; 114(9):1235–1245. [PubMed: 23264538]

Lian T, Ho RJ. Cholera toxin B-mediated targeting of lipid vesicles containing ganglioside GM1 to mucosal epithelial cells. Pharm. Res. 1997; 14(10):1309–1315. [PubMed: 9358541]

Ling EA, Wong WC. The origin and nature of ramified and amoeboid microglia: a historical review and current concepts. Glia. 1993; 7:9–18. [PubMed: 8423067]

Ling EA, Kaur LC, Yick TY, Wong WC. Immunocytochemical localization of CR3 complement receptors with OX-42 in amoeboid microglia in postnatal rats. Anat. Embryol. 1990; 182:481–486. [PubMed: 2291492]

Llado J, Haenggeli C, Pardo A, Wong V, Benson L, Coccia C, Rothstein JD, Shefner JM, Maragakis NJ. Degeneration of respiratory motor neurons in the SOD1 G93A transgenic rat model of ALS. Neurobiol. Dis. 2006; 21:110–118. [PubMed: 16084734]

Llewellyn-Smith IJ, Martin CL, Arnolda LF, Minson JB. Retrogradely transported CTB saporin kills sympathetic preganglionic neurons. Neuroreport. 1999; 10(2):307–312. [PubMed: 10203327]

Llewellyn-Smith IJ, Martin CL, Arnolda LF, Minson JB. Tracer-toxins: cholera toxin B saporin as a model. J. Neurosci. Methods. 2000; 103(1):83–90. [PubMed: 11074098]

Lovett-Barr MR, Satriotomo I, Muir G, Wilkerson JER, Hoffman MS, Vinit S, Mitchell GS. Repetitive intermittent hypoxia induces respiratory and somatic motor recovery following chronic cervical spinal injury. J. Neurosci. 2012; 32(11):3591–3600. [PubMed: 22423083]

Lujan HL, Palani G, Peduzzi JD, DiCarlo SE. Targeted ablation of mesenteric projecting sympathetic neurons reduces the hemodynamic response to pain in conscious, spinal cord-transected rats. Am. J. Physiol. Regul. Integr. Comp. Physiol. 2010; 298(5):R1358–R1365. [PubMed: 20219868]

Mantilla CB, Sieck GC. Neuromuscular adaptations to respiratory muscle inactivity. Respir. Physiol. Neurobiol. 2009; 169(2):133–140. [PubMed: 19744580]

Mantilla CB, Sieck GC. Impact of diaphragm muscle fiber atrophy on neuromotor control. Respir. Physiol. Neurobiol. 2013; 189(2):411–418. [PubMed: 23831121]

Mantilla CB, Rowley KL, Zhan WZ, Fahim MA, Sieck GC. Synaptic vesicle pools at diaphragm neuromuscular junctions vary with motoneuron soma, not axon terminal, inactivity. Neuroscience. 2007; 146(1):178–189. [PubMed: 17346898]

Mantilla CB, Zhan WZ, Sieck GC. Retrograde labeling of phrenic motoneurons by intrapleural injection. J. Neurosci. Methods. 2009; 182(2):244–249. [PubMed: 19559048]

Mantilla CB, Greising SM, Zhan WZ, Seven YB, Sieck GC. Prolonged C2 spinal hemisection-induced inactivity reduces diaphragm muscle specific force with modest, selective atrophy of type IIx and/or IIb fibers. J. Appl. Physiol. 2013; 114:380–386. [PubMed: 23195635]

McCrimmon, DR.; Mitchell, GS.; Feldman, JL.; Alheid, GF. Respiration: Network control.. In: Squire, LR., editor. Encyclopedia of Neuroscience. Academic Press; Oxford: 2009. p. 79-89.

Mitchell, GS.; McCrimmon, DR.; Feldman, JL.; Baker-Herman, TL. Respiration.. In: Squire, LR., editor. Encyclopedia of Neuroscience. Academic Press; Oxford: 2009. p. 121-130.

Navarrete-Opazo AA, Mitchell GS. Recruitment and plasticity in diaphragm, intercostal and abdominal muscles in unanesthezised rats. J. Appl. Physiol. 2014 (pii: jap. 00130.2014.).

Nichols NL, Dale EA, Mitchell GS. Severe acute intermittent hypoxia elicits phrenic long-term facilitation by a novel adenosine-dependent mechanism. J. Appl. Physiol. 2012; 112(10):1678–1688. [PubMed: 22403346]

Nichols NL, Gowing G, Satriotomo I, Nashold LJ, Dale EA, Suzuki M, Avalos P, Mulcrone PL, McHugh J, Svendsen CN, Mitchell GS. Intermittent hypoxia and stem cell implants preserve breathing capacity in a rodent model of amyotrophic lateral sclerosis. Am. J. Respir. Crit. Care Med. 2013a; 187(5):535–542. [PubMed: 23220913]

Nichols NL, Van Dyke J, Nashold L, Satriotomo I, Suzuki M, Mitchell GS. Ventilatory control in ALS. Respir. Physiol. Neurobiol. 2013b; 189(2):429–437. [PubMed: 23692930]

Nikodemova, M.; Small, AL.; Smith, SM.; Mitchell, GS.; Watters, JJ. Spinal but not cortical microglia acquire an atypical phenotype with high VEGF, galectin-3 and osteopontin, and blunted inflammatory responses in ALS rats.. Neurobiol. Dis. 2013. http://dx.doi.org/10.1016/j.nbd.2013.11.009 (pii: S0969-9961(13)00321-5)

Onimaru H, Arata A, Homma I. Localization of respiratory rhythm-generating neurons in the medulla of brainstem-spinal cord preparations from newborn rats. Neurosci. Lett. 1987; 78(2):151–155. [PubMed: 3627556]

Perrin J, Crousillat J. Splanchnic afferent input to the lateral reticular nucleus of the cat. J. Auton. Nerv. Syst. 1983; 8(4):383–393. [PubMed: 6668394]

Powers SK, Kavazis AN, Levine S. Prolonged mechanical ventilation alters diaphragmatic structure and function. Crit. Care Med. 2009; 37(10 Suppl):S347–S353. [PubMed: 20046120]

Robinson AP, White TM, Mason DW. Macrophage heterogeneity in the rat as delineated by two monoclonal antibodies MRC OX-41 and MRC OX-42, the latter recognizing complement receptor type 3. Immunology. 1986; 57:239–247. [PubMed: 3512425]

Roy A, Fung YK, Liu X, Pahan K. Up-regulation of microglial CD11b expression by nitric oxide. J. Biol. Chem. 2006; 281:14971–14980. [PubMed: 16551637]

Sherrey JH, Megirian D. After phrenicotomy the rat alters the output of the remaining respiratory muscles without changing its sleep–waking pattern. Respir. Physiol. 1990; 81(2):213–225. [PubMed: 2148218]

Shi Y, Chanana V, Watters JJ, Ferrazzano P, Sun D. Role of sodium/hydrogen exchanger isoform 1 in microglial activation and proinflammatory responses in ischemic brains. J. Neurochem. 2011; 119(1):124–135. [PubMed: 21797866]

Sieck GC. Physiological effects of diaphragm muscle denervation and disuse. Clin. Chest Med. 1994; 15:641–659. [PubMed: 7867280]

Smith JC, Ellenberger HH, Ballanyi K, Richter DW, Feldman JL. Pre-Bötzinger complex: a brainstem region that may generate respiratory rhythm in mammals. Science. 1991; 254:726–729. [PubMed: 1683005]

Smith JC, Abdala AP, Rybak IA, Paton JF. Structural and functional architecture of respiratory networks in the mammalian brainstem. Philos. Trans. R. Soc. Lond. B Biol. Sci. 2009; 364(1529):2577–2587. [PubMed: 19651658]

Trumbower RD, Jayaraman A, Mitchell GS, Rymer WZ. Exposure to acute intermittent hypoxia augments somatic motor function in humans with incomplete spinal cord injury. Neurorehabil. Neural Repair. 2012; 26:163–172. [PubMed: 21821826]

Vinit S, Windelborn JA, Mitchell GS. Lipopolysaccharide attenuates phrenic long-term facilitation following acute intermittent hypoxia. Respir. Physiol. Neurobiol. 2011; 176(3):130–135. [PubMed: 21334467]

Watson, C.; Paxinos, G.; Kayalioglu, G. The Spinal Cord: A Christopher and Dana Reeve Foundation Text and Atlas. Academic Press; London: 2009.

Windelborn JA, Mitchell GS. Glial activation in the spinal ventral horn caudal to cervical injury. Respir. Physiol. Neurobiol. 2012; 180(1):61–68. [PubMed: 22041654]

Zaidi SI, Jafri A, Doggett T, Haxhiu MA. Airway-related vagal preganglionic neurons express brain-derived neurotrophic factor and TrkB receptors: implications for neuronal plasticity. Brain Res. 2005; 1044(2):133–143. [PubMed: 15885212]

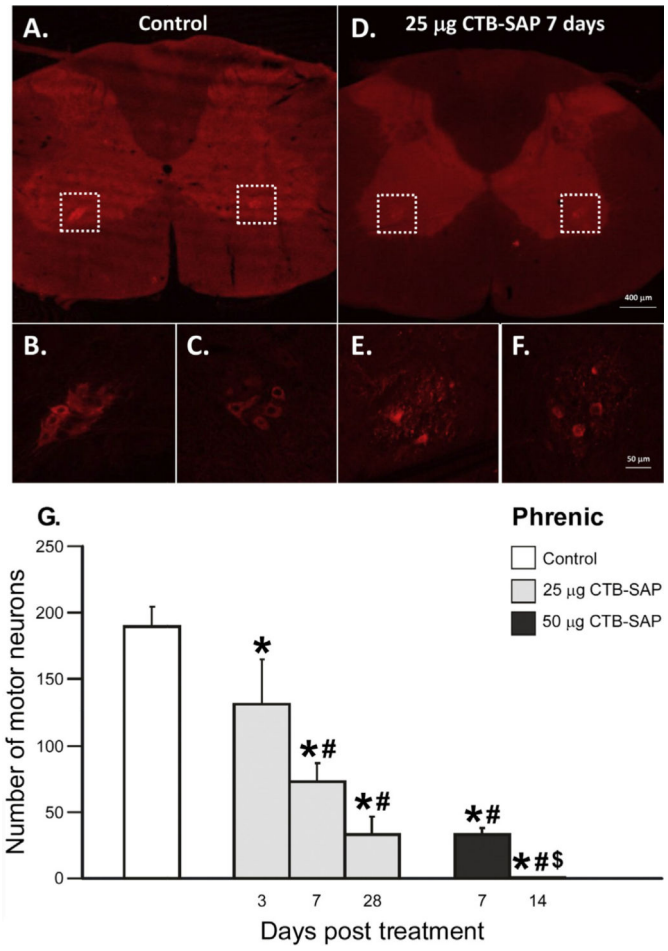

Fig. 1.

Phrenic motor neuron survival in CTB–SAP treated rats. A–F. Photomicrographs (4× A and D; 20× B, C, E, and F) depicting representative CTB stained sections from the C3–5 spinal ventral horn from a control rat (A–C), and a 25 µg CTB–SAP treated rat at 7 days (D–F). Framed regions in A and D are shown at higher magnification (20×) in B, C, E, and F. Notice the number and shape of healthy, pyramidal-shaped CTB(+) labeled phrenic motor neurons in the control rat (A–C) *versus* the paucity of surviving phrenic motor neurons after CTB–SAP treatment (D–F). G. CTB–SAP dose response of phrenic motor neuron survival. Phrenic motor neuron survival in control rats (CTB + SAP; white bar) and rats injected with either 25 (light gray bars) or 50 µg (dark gray bars) CTB–SAP at 3, 7, 14 or 28 days post-injection. Phrenic motor neuron survival is significantly decreased in all CTB–SAP treated *versus* control rats (*; $p < 0.05$). Rats at 3 days post-25 µg CTB–SAP had significantly greater phrenic motor neuron survival *versus* all other CTB–SAP treated rats (#; $p < 0.05$). Rats at 7 days post-25 µg CTB–SAP had greater phrenic motor neuron survival *versus* rats 14 days post-50 µg CTB–SAP ($; $p < 0.05$). Means ± 1 SEM. Scale bar at 4× = 400 µm, 20×= 50 µm.

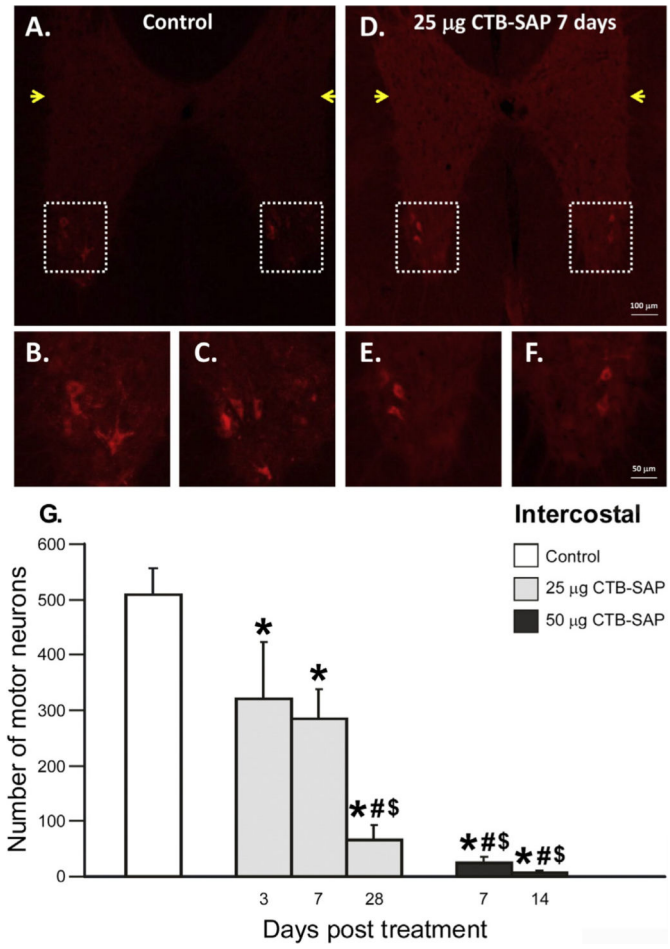

Fig. 2.

Intercostal motor neuron survival in CTB–SAP treated rats. A–F. Photomicrographs (10× A and D; 20× B, C, E, and F) depicting representative CTB stained sections from the T2–7 spinal ventral horn in a control rat (A–C) and a rat 7 days post-25 µg CTB–SAP (D–F). Framed regions in A and D are shown at higher magnification (20×) in B, C, E, and F. Yellow arrows are pointing towards the intermediolateral cell column, in which there is a lack of staining. G. CTB–SAP dose response of intercostal motor neuron survival. Intercostal motor neuron survival in control rats (CTB + SAP; white bar) and rats injected with either 25 (light gray bars) or 50 µg (dark gray bars) CTB–SAP at 3, 7, 14, or 28 days post-injection. Intercostal motor neuron survival is significantly decreased in all CTB–SAP treated rats *versus* control rats (*; $p < 0.05$). Rats 3 days post-25 µg CTB–SAP had significantly greater intercostal motor neuron survival *versus* rats 28 days post-25 µg CTB–SAP and 7 or 14 days post-50 µg CTB–SAP (#; $p < 0.05$). Rats at 7 days post-25 µg CTB–SAP had significantly greater intercostal motor neuron survival *versus* rats 28 days post-25 µg CTB–SAP and 7 or 14 days post-50 µg CTB–SAP ($; $p < 0.05$). Means ± 1 SEM. Scale bar at 10× = 100 µm, 20× = 50 µm.

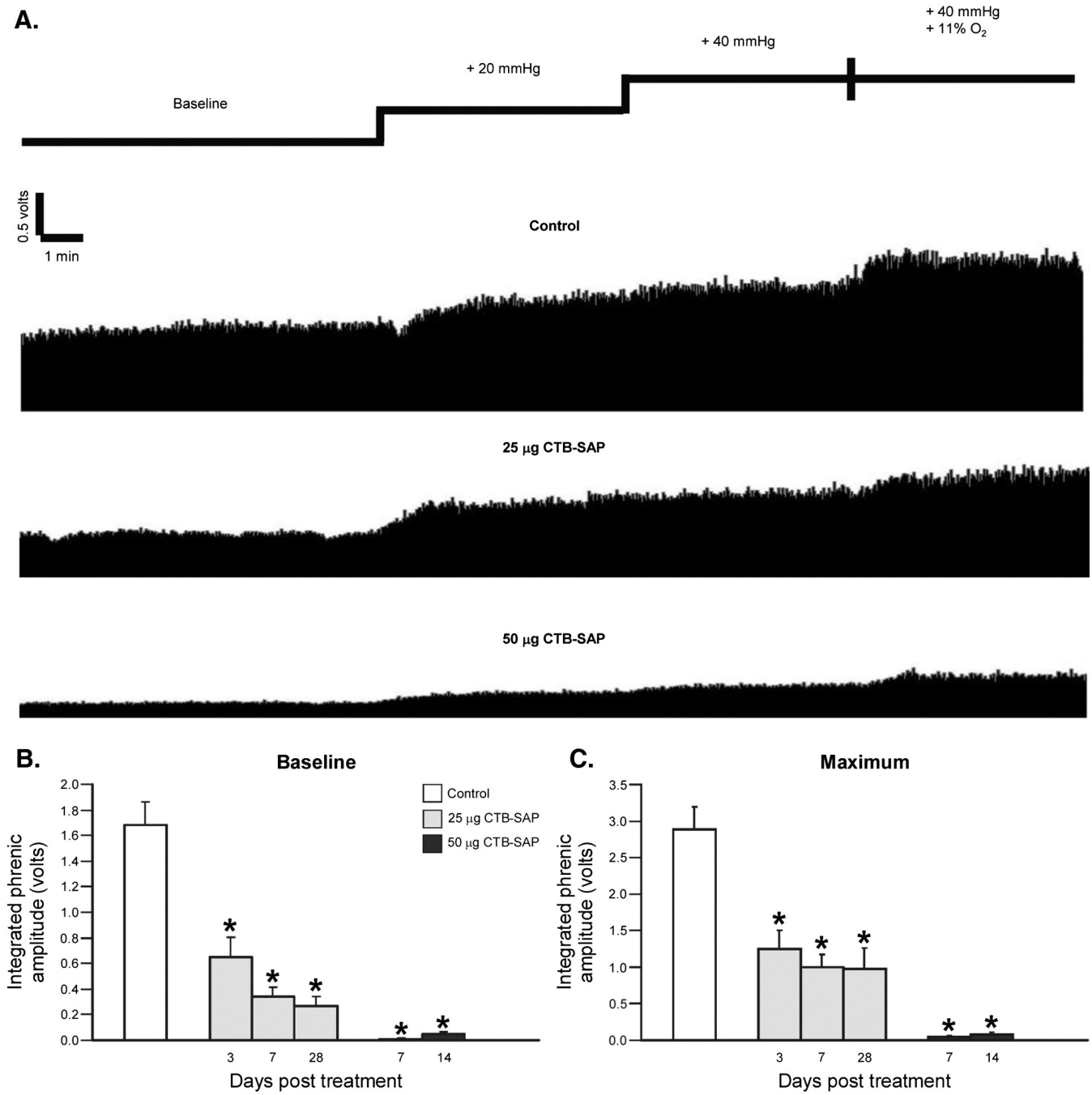

Fig. 3.

Phrenic motor output in control and CTB–SAP treated rats. A. Representative traces of integrated phrenic neurograms in control (CTB + SAP) rats and in rats following 25 or 50 µg CTB–SAP. Spontaneous phrenic activity was recorded in all rats at baseline, and then during 5 min of hypercapnia (20 and 40 Torr CO_2 increase), followed by a maximal response to hypercapnia (40 Torr CO_2 increase) + hypoxia (11% O_2). Phrenic motor output during baseline and the maximal response were compared in B and C. Integrated phrenic amplitude at baseline (B) and in response to maximal chemoreceptor stimulation (C) for control rats

(CTB + SAP; white bar) and rats injected with either 25 (light gray bars) or 50 μg (dark gray bars) CTB–SAP. Phrenic motor output at baseline and in response to maximal chemoreceptor stimulation was significantly reduced in all CTB–SAP treated *versus* control rats (*; $p < 0.05$). Means ± 1 SEM.

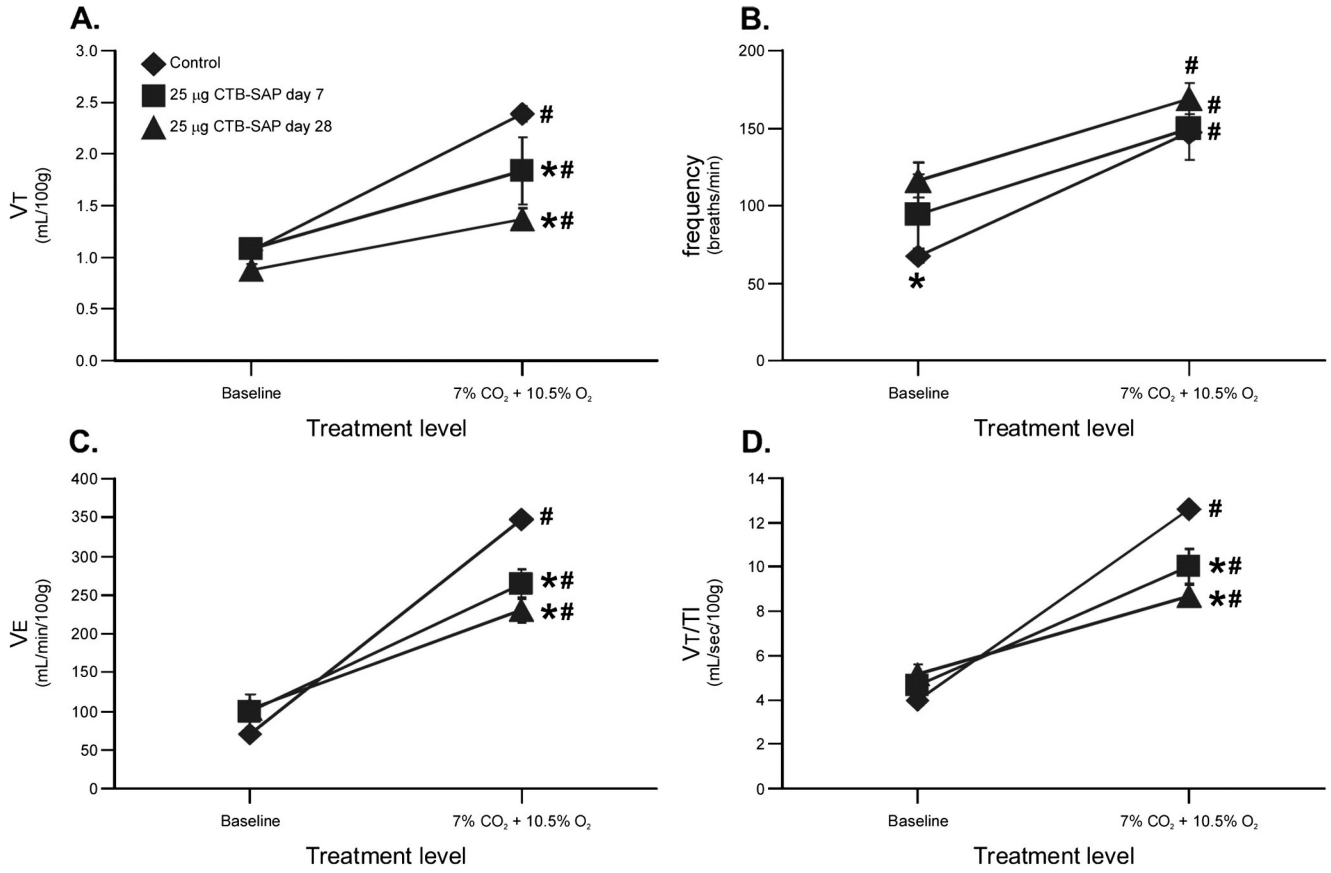

Fig. 4.

Respiratory variables in unanesthetized control and CTB–SAP treated rats. Respiratory variables including tidal volume (VT; A), breathing frequency (B), minute ventilation ($\dot{V}E$; C) and mean inspiratory flow (VT/TI; D) at baseline and in response to hypercapnia + hypoxia (7% CO_2 + 10.5% O_2) in rats following control (CTB + SAP; diamonds) or 25 μg CTB–SAP at 7 (squares) or 28 (triangles) days post-injection. All breathing volumes (VT, $\dot{V}E$, and VT/TI) were normalized per 100 g of body mass. VT, $\dot{V}E$ and VT/TI were not affected at baseline by CTB–SAP, but were slightly decreased in response to 7% CO_2 + 10.5% O_2 in CTB–SAP treated *versus* control rats (*; $p < 0.05$). Baseline frequency was significantly increased only with 25 μg CTB–SAP at 28 days post-treatment *versus* control rats (*; $p < 0.05$). In all rats, there was in increase in VT, frequency, $\dot{V}E$ and VT/TI during 7% CO_2 + 10.5 O_2 (#; $p < 0.05$). Means ± 1 SEM.

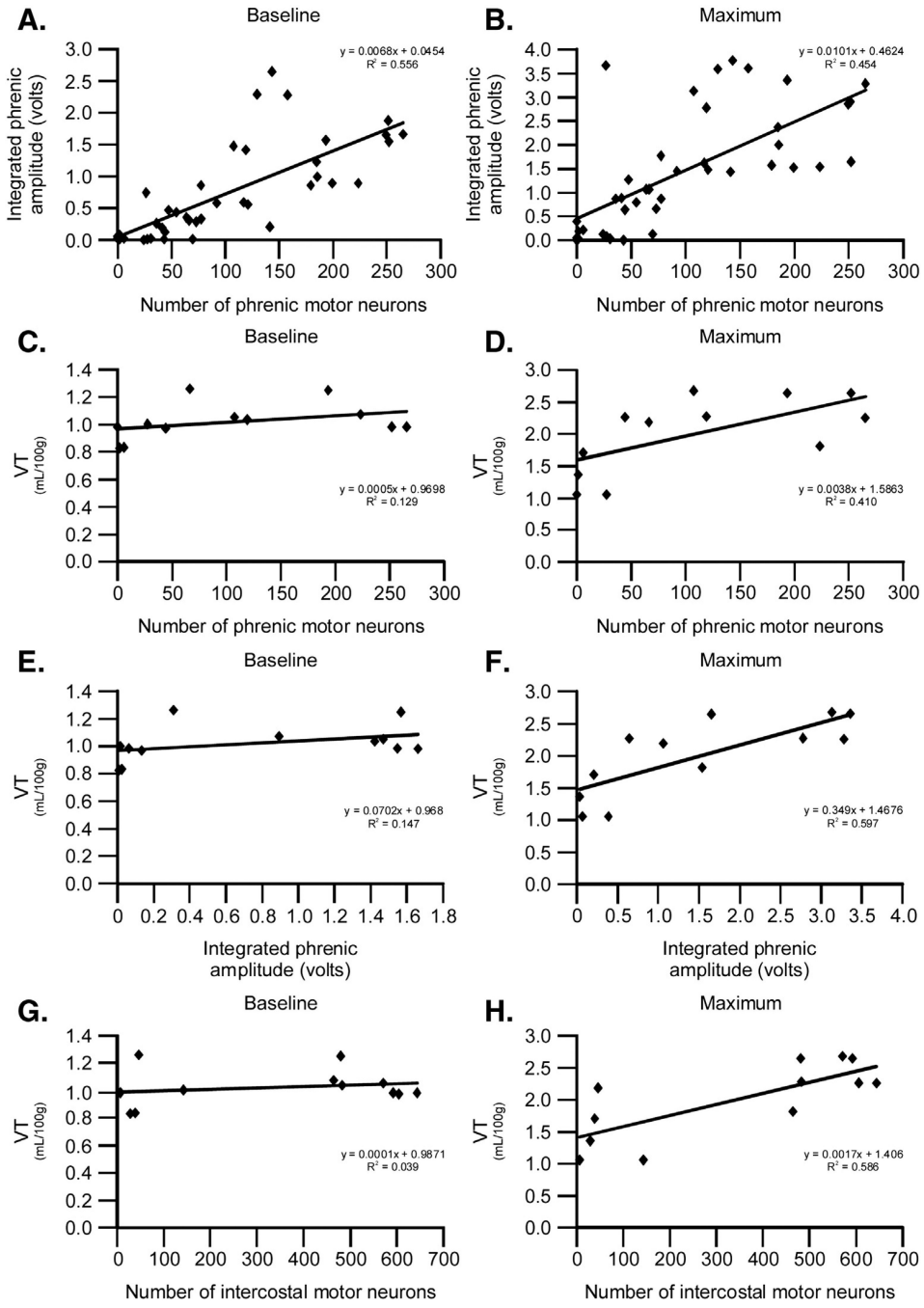

Fig. 5.

Regression analyses reveal significant correlations. Multiple regression analyses between baseline or maximal phrenic output with phrenic motor neuron survival (A, B), baseline or maximal VT/100 g with phrenic motor neuron survival (C, D), baseline or maximal VT/100 g with baseline or maximal phrenic output (E, F), and baseline or maximal VT/100 g with intercostal motor neuron survival (G, H). Significant correlations exist between baseline or maximal phrenic output with phrenic motor neuron survival ($p < 0.001$), maximal VT/100 g with phrenic motor neuron survival ($p = 0.025$), maximal VT/100 g with maximal phrenic

output ($p = 0.003$), and maximal VT/100 g with intercostal motor neuron survival ($p = 0.004$). Thus, phrenic motor neuron survival predicts phrenic motor output and maximal VT/100 g, maximal phrenic motor output predicts maximal VT/100 g, and intercostal motor neuron survival predicts maximal VT/100 g.

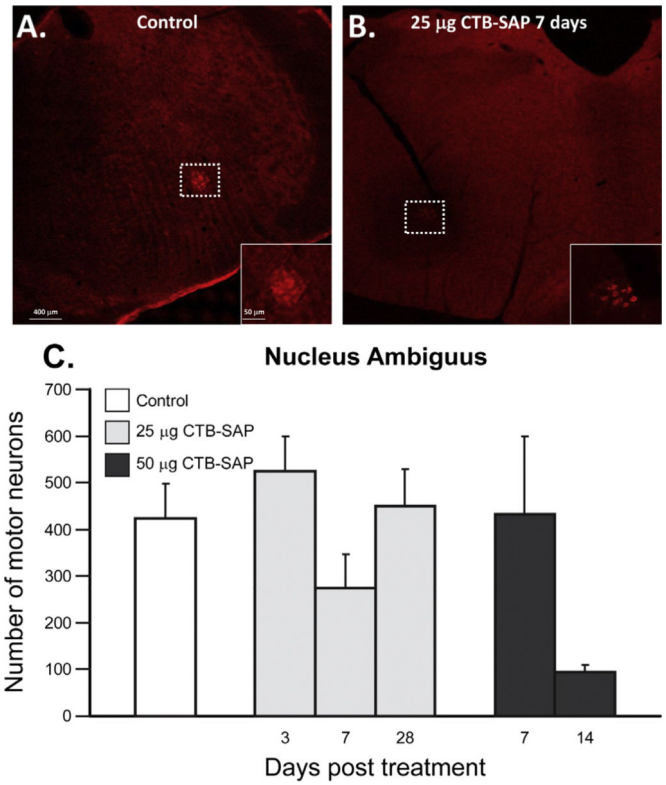

Fig 6.

Nucleus Ambiguus cell numbers in control and CTB–SAP treated rats. A, B. Photomicrographs (4×) depicting representative CTB stained sections from the brainstem in a control rat (A), and a rat 7 days post-25 µg CTB–SAP (B). Framed regions in A and B are shown at higher magnification in the lower right hand panels (20×). C. Nucleus Ambiguus motor neuron survival in control rats (CTB + SAP; white bar) and rats 3, 7, 14, or 28 days post-25 (light gray bars) or 50 µg (dark gray bars) CTB–SAP. Nucleus Ambiguus motor neuron survival is unchanged by CTB–SAP. Means ± 1 SEM. Scale bar at 4× = 400 µm, 20× = 50 µm.

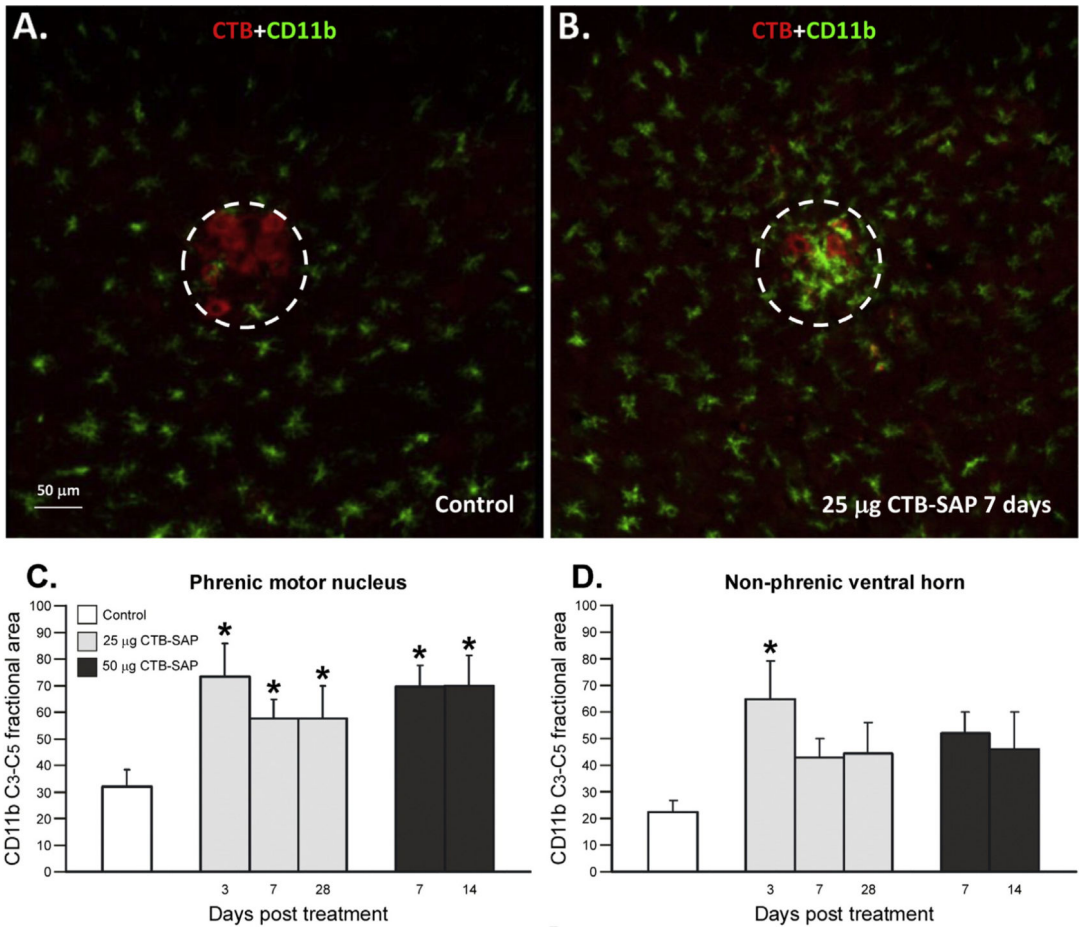

Fig. 7.

CD11b fractional area is increased in the phrenic motor nucleus after CTB–SAP. A, B. Photomicrographs (20×) depicting representative CTB (red; phrenic motor neurons) and CD11b (green; microglial marker) stained sections from the C3–5 spinal ventral horn from a control rat (A) and 7 days post-25 μg CTB–SAP (B). The phrenic motor nucleus is circumscribed by the dashed, white circle in A and B. Notice, increased CD11b staining in the phrenic motor nucleus of a CTB–SAP treated *vs.* control rat. C and D. CD11b C3–5 fractional area in control rats (CTB + SAP; white bar) and rats injected with either 25 (light gray bars) or 50 μg (dark gray bars) CTB–SAP at 3, 7, 14, or 28 days post-injection in the phrenic motor nucleus (C), and the non-phrenic ventral horn in the same spinal segments (D). CD11b C3–5 fractional area in the phrenic motor nucleus is significantly increased in all CTB–SAP treated *versus* control rats (*; $p < 0.05$). CD11b C3–5 fractional area in the non-phrenic ventral horn is only significantly increased 3 days post-25 μg CTB–SAP *versus* control (*; $p < 0.05$). Means ± 1 SEM. Scale bar at 4× = 400 μm, 20× = 50 μm. (For interpretation of the references to color in this figure legend, the reader is referred to the web version of this article.)